Superlattices and Microstructures, Vol. 23, No. 3/4, 1998

Magnetotransport in a periodic composite medium: New phenomena in a classical physics context

DAVID J. BERGMAN, YAKOV M. STRELNIKER
School of Physics and Astronomy, Raymond and Beverly Sackler Faculty of Exact Sciences, Tel Aviv University, Tel Aviv 69978, Israel

(Received 30 September 1997)

The magnetotransport properties of a composite conductor with a periodic microstructure have recently been studied both theoretically and numerically using a local classical continuum physics description of the transport at the microscale. Surprising new phenomena were discovered, including an induced magnetoresistance which oscillates strongly when the magnetic field is sufficiently strong and is rotated with respect to the microstructure. A surprising aspect of this phenomenon is that the effect is much stronger when the microstructure is two dimensional than when it is three dimensional. The physical reasons for this are discussed. Briefly, this is concerned with the question of whether the current distribution saturates with increasing strength of the magnetic field. In two-dimensional metal-insulator microstructures, the magnetoresistance usually does not saturate. But when it does, some components of the local current distribution must exhibit a surprising degree of uniformity over the conducting constituent.

Key words: magnetotransport, magnetoresistance, composite medium.

1. Introduction

It is often assumed that any interesting new phenomena in solid materials must have their origins in quantum behavior. The rationalization which underlies this prejudice is that such materials have been studied for so long that all the important phenomena which can arise in the context of a classical continuum physics picture have already been discovered. A recent example that belies this expectation are the surprising magnetotransport properties of composite conductors which have a periodic microstructure [1].

When different homogeneous conductors are mixed together to make a macroscopically inhomogeneous or composite medium, the bulk effective transport properties will usually include a non-vanishing magnetoresistance, even when each component is either a simple free-electron conductor or a perfect insulator. This can be understood as follows. When a prescribed average (i.e., volume average) current density $\langle \boldsymbol{J} \rangle$ is made to flow through the composite medium, the local current density $\boldsymbol{J}(\boldsymbol{r})$ is usually non-uniform, and its magnitude as well as its direction vary from point to point. Therefore, in the presence of an external magnetic field $\boldsymbol{B}$, the local electric Hall field $\boldsymbol{E}_H \propto (\boldsymbol{B} \times \boldsymbol{J})$ usually has a non-vanishing component along $\langle \boldsymbol{J} \rangle$. The bulk effective ohmic resistivity ρ_e in the direction of $\langle \boldsymbol{J} \rangle$ is found from

$$\rho_e \equiv \frac{\langle \boldsymbol{J} \rangle \cdot \langle \boldsymbol{E} \rangle}{\langle \boldsymbol{J} \rangle^2}. \tag{1.1}$$

0749–6036/98/030547 + 11 $25.00/0 sm970522

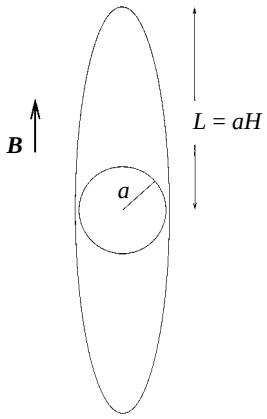

Fig. 1. Cigar-shaped region of strong current distortion near a spherical inclusion.

Therefore, ρ_e will acquire a dependence on $\boldsymbol{B}$ if the average of $\boldsymbol{E}_H$ has a non-zero component along $\langle \boldsymbol{J} \rangle$. It turns out that, although to leading order in $\boldsymbol{B}$ that component of $\langle \boldsymbol{E}_H \rangle$ vanishes, it has non-vanishing contributions at all even orders, beginning with $\mathcal{O}(\boldsymbol{B}^2)$.

When $\boldsymbol{B}$ is strong enough so that the Hall resistivity ρ_H of a uniform conductor is greater than its ohmic resistivity ρ_0, then the presence of inclusions leads to the appearance of a new class of physical phenomena. The problem of a single isolated inclusion of spherical or ellipsoidal shape under a uniform applied electric field $\boldsymbol{E}_0$ is essentially solvable in closed form, even when the two materials are anisotropic conductors, and even when the resistivity tensors are non-symmetric†. An important feature of the solution, in the case where $\rho_H \gg \rho_0$, is that the spatial region where $\boldsymbol{J}(\boldsymbol{r})$ is strongly distorted is no longer confined to the close vicinity of the inclusion. Instead it now has a shape that is elongated in the directions of $\pm\boldsymbol{B}$ (see Fig. 1). The region of strong distortion is roughly cigar shaped, with the inclusion at its center, determining its lateral dimensions. The half length L of the cigar-shaped region is roughly equal to the linear size a of the inclusion multiplied by an enhancement factor

$$L \cong |H|a, \quad H \equiv \frac{\rho_H}{\rho_0}. \tag{1.2}$$

Of course, the cigar-shaped region of strong distortion is not sharply defined for any finite value of H. Nevertheless, its boundaries become asymptotically sharp as $H \to \pm\infty$. The physical length L and the Hall-to-ohmic resistivity ratio H play important roles in the subsequent discussion. It is worth noting that $H = \mu|\boldsymbol{B}|$, where μ is the Hall mobility. Also, in a free-electron conductor we have $H = \omega_c\tau$, where $\omega_c \equiv e|\boldsymbol{B}|/mc$ is the cyclotron frequency of the charge carriers, while τ is the charge transport relaxation time. We note that both μ and ω_c have the same sign as the electric charge e of the charge carriers.

The distortion of the local current density field leads, as usual, to enhanced dissipation, and consequently to an increased total resistance. Because the cigar-shaped volume of strong distortion is proportional to $|H|$, the extra dissipation also exhibits such a dependence, and thus the ohmic resistance increases with $\boldsymbol{B}$, roughly in proportion to $|\boldsymbol{B}|$ and without any saturation. Of course, when there is a finite density of such inclusions, then the expanding distortion cigar will eventually begin to overlap, and therefore interact, with the distortion cigars of other inclusions. This is similar to the situation when an incident plane wave is scattered by different localized scatterers, and multiple scattering begins to be important.

† This fact is apparently known to many people, but we are unaware of a published proof. Such a proof will appear in a review article that is currently in preparation.

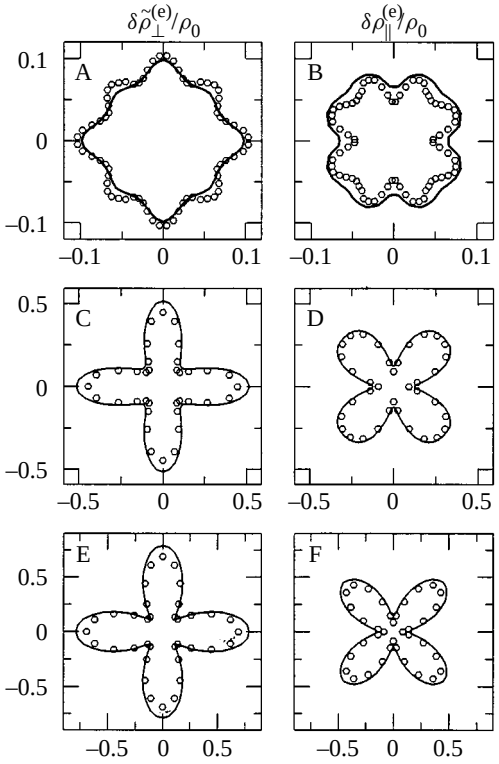

Fig. 2. Polar plots of $\delta\rho_{\parallel}^{(e)}(\boldsymbol{B})/\rho_0$ and $\delta\tilde{\rho}_{\perp}^{(e)}(\boldsymbol{B})/\rho_0$ for the three investigated antidot radii at the highest magnetic field, $|\boldsymbol{B}| = 12$ T, i.e., $H = \mu|\vec{B}| = 3$. Experimental points are shown as open circles, theoretical fits as full lines. From top to bottom the geometrical antidot radii are: A, B, $R_{\text{geom}} = 55$ nm; C, D, $R_{\text{geom}} = 110$ nm; E, F, $R_{\text{geom}} = 130$ nm. The fitted cylinder radii, used in the calculations, were 73, 180, and 215 nm, respectively, and a normalized effective film thickness of $h/a = 0.45$ was also used instead of the lithographic value $h/a = 300$ nm$/500$ nm $= 0.6$ (after [1]).

When the inclusions are identical and form a periodic array, then the interactions between overlapping distortion cigars result in some surprising behavior, which was unforeseen until quite recently. When $|H| \gg 1$ then, because the region of strong distortion around an isolated inclusion is sharply defined, two such regions can only overlap if $\boldsymbol{B}$ is roughly parallel to their separation vector, and if $2L$ is greater than the separation between the two inclusions. Consequently, the magnitude of $\boldsymbol{B}$ at which distortions produced by different inclusions begin to interact will depend not only on the inclusion sizes, but also on the direction of $\boldsymbol{B}$. These interactions can lead either to enhancement or attenuation of the dissipation rate, thus the bulk effective magnetoresistance exhibits a strongly oscillatory behavior as $\boldsymbol{B}$ is rotated with respect to the periodic microstructure. Such behavior was first found in detailed numerical calculations of the magnetoresistance in such systems [2], then its physical origins were understood, as explained here [2], and finally the phenomenon was observed experimentally, in good quantitative agreement with the detailed calculations [1] (see Fig. 2).

One of the surprising aspects of this strongly anisotropic induced magnetoresistance is that it looks remarkably similar to the magnetoresistance observed at liquid helium temperatures in clean single crystals of transition metals such as copper and gold. This can be seen from Fig. 3, where we show, side by side, the results of some old measurements on copper [3], and of our own calculations on a classical fcc array of perfectly insulating spheres embedded in a uniform, free-electron conducting host [2]. Note that, whereas

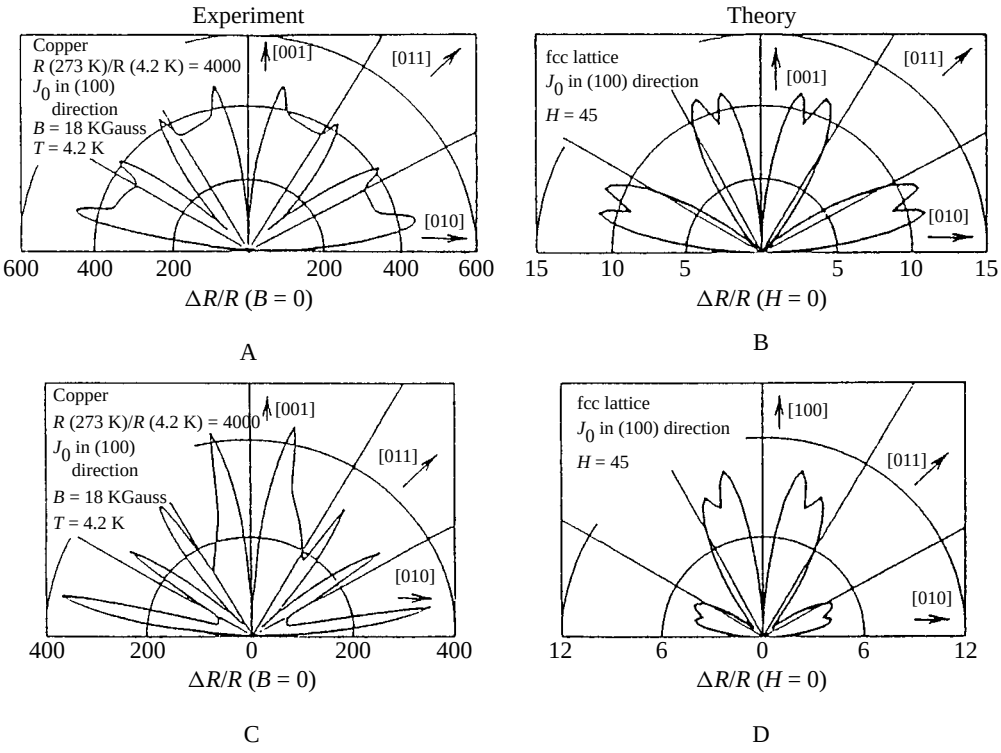

Fig. 3. Relative transverse magnetoresistance $\delta\rho_\perp/\rho_0$ in a fixed direction as a function of the magnetic field direction. In A and B the magnetic field is rotated in the plane perpendicular to the (100) axis, while in C and D it is rotated in the plane perpendicular to an axis inclined less than 3° away from the (100) axis. The results plotted on the left side, A and C, are real experimental data obtained for copper at 18000 Gauss and 4.2 K in [3], while the plots on the right side are our own results, obtained by numerical computation for an fcc lattice of spherical inclusions. The striking difference between the two pairs of figures, A and B, and C and D, is a result of the great sensitivity to sample orientation, as found both in the experiment [3] and in our calculations (after [2]).

the behavior of copper is known to result from the special shape of its Fermi surface, which is non-compact and supports extended orbits for the $\boldsymbol{k}$-space motion of charge carriers in the presence of a $\boldsymbol{B}$-field [4], our model is not only completely devoid of any quantum elements like $\boldsymbol{k}$-space and Fermi surface, but it does not even require the existence of discrete charge carriers. The model only assumes that the local current density is determined by the local electric field $\boldsymbol{E}(\boldsymbol{r}) \equiv \nabla\phi(\boldsymbol{r})$ and conductivity tensor $\hat{\sigma}(\boldsymbol{r}) = 1/\hat{\rho}(\boldsymbol{r})$ at that same point. All we have to do in order to find the bulk effective conductivity tensor $\hat{\sigma}_e = 1/\hat{\rho}_e$ is to solve some boundary-value problems based upon the continuity equation for the local current density $\boldsymbol{J}(\boldsymbol{r})$

$$\begin{aligned} \nabla \cdot \boldsymbol{J}^{(\beta)} &\equiv \nabla \cdot \hat{\sigma} \cdot \nabla\phi^{(\beta)} = 0, \qquad r \in V, \\ \phi^{(\beta)}(\boldsymbol{r}) &= r_\beta, \qquad r \in \partial V, \end{aligned} \tag{1.3}$$

where r_β is the β-component of $\boldsymbol{r}$, and then calculate the volume average of $\boldsymbol{J}^{(\beta)}$

$$\sigma^{(e)}_{\alpha\beta} = \langle J^{(\beta)}_\alpha(\boldsymbol{r})\rangle = \sum_\gamma \langle \sigma_{\alpha\gamma}(\boldsymbol{r})\partial_\gamma\phi^{(\beta)}(\boldsymbol{r})\rangle. \tag{1.4}$$

Consequently, whereas observation of the oscillatory anisotropic behavior of ρ_e in the case of copper or gold requires very pure single crystals and liquid helium temperatures, the observation of similar behavior in a periodic composite only requires that the Hall mobility μ and magnetic field $\boldsymbol{B}$ be large enough so that

$|H| = |\mu \boldsymbol{B}| \geq 1$. This can be achieved at much higher temperatures, and using doped semiconductors instead of pure metallic single crystals [1].

It should be stressed that, despite the qualitative similarities of the angular ρ_e vs. $\boldsymbol{B}$ plots (see Fig. 3), the classical model can not be applied to a description of copper or gold. The sizes of the ionic cores in those crystals are not larger than the de Broglie wavelengths of the charge carriers, and the ionic cores are also much smaller than the mean free paths of those charge carriers. Thus, a classical continuum physics description of the transport behavior on the microscale is out of the question. However, using state of the art technology, arrays of mesoscopic quantum dots or antidots can be fabricated today where those parameters can be adjusted so that the inhomogeneity length scale is larger than both the quantum and kinetic length scales. For such systems, the classical continuum description is the correct first approximation, as shown by the work described in [1].

2. Two-dimensional versus three-dimensional microstructures

Numerical calculations have already been carried out on various structures, including three-dimensional (3D) simple-cubic and face-centered-cubic arrays of insulating spheres and two-dimensional (2D) square arrays of insulating cylinders embedded in a free-electron-like conducting host [2, 5]. In order to do this, special numerical methods were developed for solving (1.3) in a periodic composite when $|H| \gg 1$ [6]. A remarkable conclusion from those calculations is that the magnitude of the effect is much larger in 2D systems than in 3D systems. This is evident from Figs 4A and 5A, which show results for a sphere array and a cylinder array, respectively, with the same radius and the same value of H, and also from comparing the results in the two pairs of figures 4B and 5D, and 4C and 5G. Moreover, the anisotropy of ρ_e for the cylinder array becomes more and more pronounced with increasing $|H|$ (compare, respectively, the figures in the following three sequences: Figs 5A–C, 5D–F and 5G–I. This is due to the fact that the value of ρ_e at its maxima seems to be increasing like H^2, whereas at the minima it remains constant.

In the case of 2D microstructures, the behavior described above is found only when $\boldsymbol{B}$ has a non-vanishing component that is perpendicular to the cylindrical symmetry axis [2]. By contrast, when $\boldsymbol{B}$ lies along that axis, it can easily be shown that the local current density, although distorted by the presence of insulating inclusions, is unaffected by the presence of a magnetic field. Consequently, the bulk effective Hall resistivity of such a configuration is the same as that of the conducting host [7], and the relative magnetoresistance is also the same as that of the conducting host [8] (e.g., it vanishes if the host is a free-electron conductor). These properties hold for a strictly 2D system, i.e., for a vanishingly thin film that is perpendicular to $\boldsymbol{B}$, as well as for a 3D system with a 2D microstructure, i.e., for a film of finite or infinite thickness that is perpendicular to $\boldsymbol{B}$.

By contrast, the induced magnetoresistance that we found in 2D microstructures requires not only that $\boldsymbol{B}$ have a non-vanishing component in the film plane, but also that the film thickness be not too small. More precisely, the film thickness h and the inhomogeneity length scale a must satisfy $H > a/h$ (see [5]).

The fact that there is a *qualitative difference* in behavior between 3D and 2D systems was emphasized by performing calculations on a sequence of 3D, simple-cubic arrays of *finite cylinders*. Every cubic unit cell, with an edge equal to 1, had at its center an insulating inclusion in the shape of a cylinder of radius $a < 0.5$ and length $l \leq 1$, which was oriented along the x-axis of the cell. It was found that, as long as l was strictly less than 1, even by very little, the magnitude of the in-plane transverse resistivity $\tilde{\rho}_{\perp}^{(e)}$ (for a precise definition of $\rho_{\perp}^{(e)}$, $\tilde{\rho}_{\perp}^{(e)}$, $\rho_{\parallel}^{(e)}$ see Fig. 5 caption) at its maxima tended to saturate with increasing $|H|$. But when $l = 1$, i.e., when the finite cylinders combined to form a 2D square array of *infinitely long cylinders*, then the behavior of $\tilde{\rho}_{\perp}^{(e)}$ with increasing $|H|$ changed drastically: instead of levelling off when $|H|$ became large, the value of $\tilde{\rho}_{\perp}^{(e)}$ at its maxima continued to increase roughly as H^2 for as long as we were able to calculate it (see Fig. 6)!

In order to try to understand this behavior, we first recall a result from a previous study of magnetotransport in a 3D Sierpińsky gasket. When a fixed external or macroscopic current was fed into the system, the

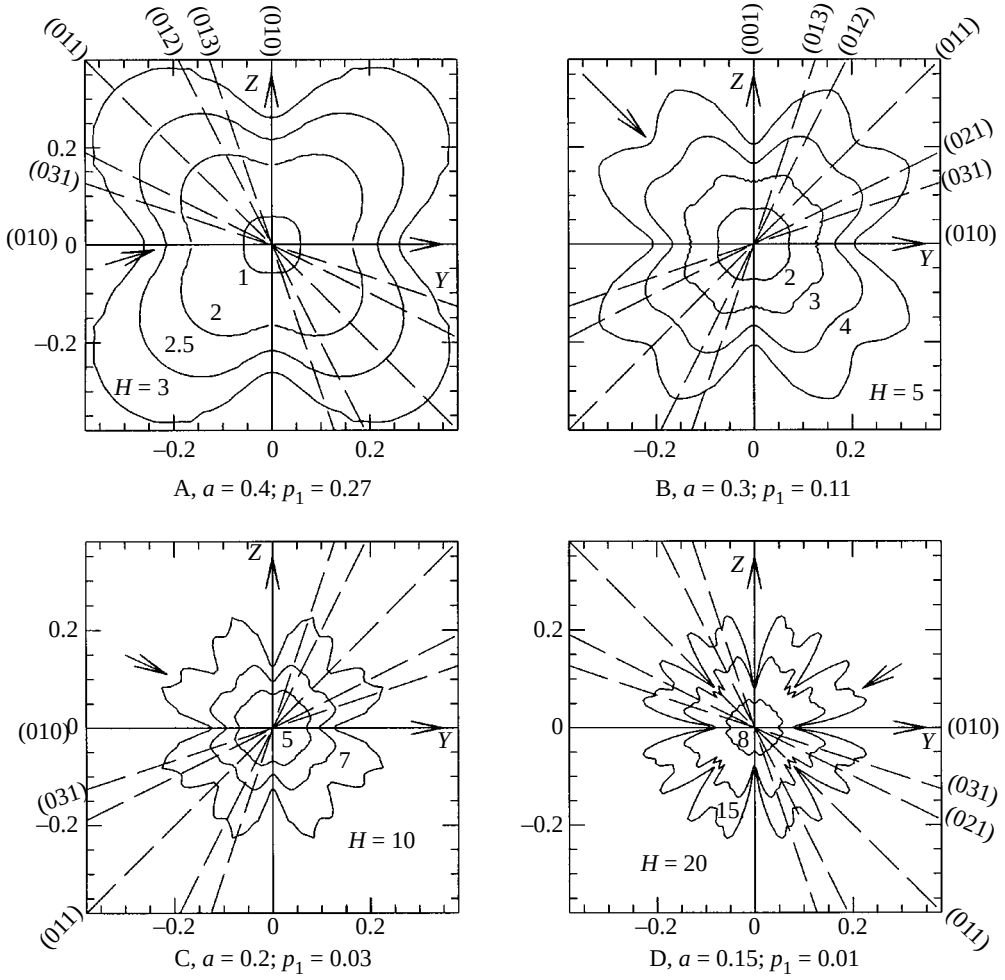

Fig. 4. Polar plots of the transverse magnetoresistance $\rho_{\perp}^{(e)} \equiv \rho_{xx}^{(e)}(\boldsymbol{B})$ for four samples of a cubic array of insulating spheres with radii $a = 0.40, 0.30, 0.20, 0.15$ and a lattice constant equal to 1, embedded in a free-electron host medium. The volume fraction of the spheres, p_1, is shown in the figure. The relative transverse magnetoresistance $\delta\rho_{\perp}^{(e)}/\rho_0 \equiv \rho_{xx}^{(e)}(\boldsymbol{B})/\rho^{(e)}(\boldsymbol{0}) - 1$ is plotted for fixed $|\boldsymbol{B}|$ as a function of the direction of $\boldsymbol{B}$ in the y, z-plane. The magnitudes listed for H are actually the values of the dimensionless Hall-to-ohmic resistivity ratio, ρ_{xy}/ρ_{xx}, for the metallic host medium. We recall that $H = \mu|\boldsymbol{B}|$ for a free-electron conductor. The maximum number of minima in $\delta\rho_{\perp}^{(e)}/\rho_0$ increases by 1 along a new lattice axis each time the sphere radius is decreased along the sequence of values corresponding to the four samples of this figure. The new minimum which appears in each sample is highlighted by an arrow. The jagged oscillations which are evident in a few places in A and B are due to calculational errors. The reciprocal lattice vectors used in these calculations ranged from -7 to 7 in each direction (after [2]).

current distribution on length scales, small compared with a characteristic magnetic-field-dependent length ξ_H, was independent of H [9, 10]. We conjecture that the analog of this behavior also appears in the periodic microstructures, where instead of an hierarchy of microstructural length scales there is usually just one length scale a or 1 (i.e., the obstacle size or the unit-cell size), or at most a small finite number of such scales. Here, too, we think that the local current distribution becomes independent of H (i.e., it is saturated) when $L = a|H| \gg 1$. This idea would explain why ρ_e saturates in 3D microstructures, since the local rate of

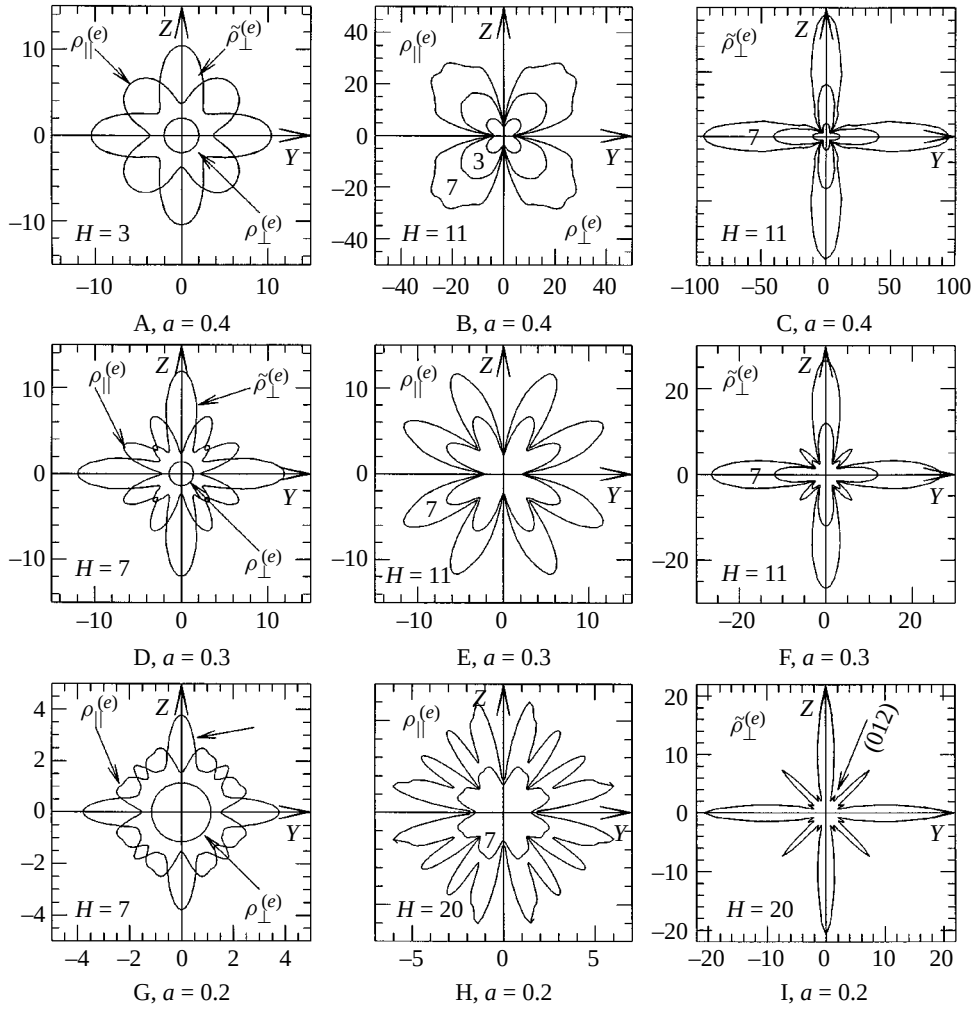

Fig. 5. Polar plots of the absolute magnetoresistance (the components $\rho_{\perp}^{(e)}, \rho_{\parallel}^{(e)}, \tilde{\rho}_{\perp}^{(e)}$) vs. the direction of $\boldsymbol{B}$ in the y, z-plane for three samples, each of them consisting of a 2D cubic array of infinitely long, perfectly insulating circular cylinders, with axes in the x-direction and radii $a = 0.4, 0.3, 0.2$, embedded in a free-electron conducting host. The component $\rho_{\perp}^{(e)}(\langle \boldsymbol{J} \rangle \| x$ along the cylinder axes and $\boldsymbol{B} \perp x$ in the y, z-plane) has no field dependence and is entirely isotropic (see the circle in the centers of A, D and G. The other two components ($\langle \vec{J} \rangle \perp x$ perpendicular to the cylinder axes: $\langle \vec{J} \rangle \| \vec{B}$ for the longitudinal resistivity $\rho_{\parallel}^{(e)}$, $\langle \boldsymbol{J} \rangle \perp \boldsymbol{B}$ for the in-plane transverse resistivity $\tilde{\rho}_{\perp}^{(e)}$) exhibit strong angular dependences. In the first column A, D and G all three components are shown for a single value of H, while in the second column B, E and H only $\rho_{\parallel}^{(e)}$ is shown, but for different values of H, and in the third column C, F and I only $\tilde{\rho}_{\perp}^{(e)}$ is shown, again for different values of H. The number of minima (for $\rho_{\parallel}^{(e)}$) or maxima (for $\tilde{\rho}_{\perp}^{(e)}$) increases by one along a new lattice axis each time the cylinder radius is decreased. Note that the small maxima in the (012)-like directions in I, one of which is marked by an arrow, are *real*. The reciprocal lattice vectors used in these calculations ranged from -10 to 10 in each direction (after [2]).

dissipation W, given by

$$W = \rho_{xx} J_x^2 + \rho_{yy} J_y^2 + \rho_{zz} J_z^2, \tag{2.1}$$

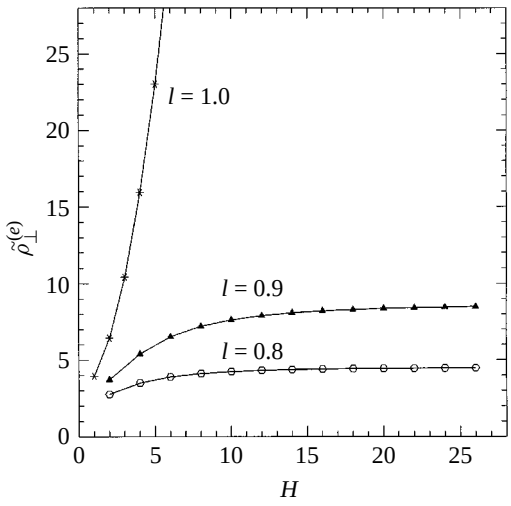

Fig. 6. The y, z-plane transverse effective resistivity $\tilde{\rho}_\perp^{(e)}$ of three samples of cylinder arrays of lengths (in the x-direction) $l = 0.8, 0.9, 1.0$ (the last case corresponds to infinitely long cylinders) as a function of the strength of the magnetic field H, which is always directed along the (010) axis. For cylinders of finite length, $\tilde{\rho}_\perp^{(e)}$ saturates as $H \to \infty$, but when that length is infinite, $\tilde{\rho}_\perp^{(e)}$ continues to increase without limit, approximately as H^2. The reciprocal lattice size was the same as in Fig. 5 (after [2]).

can depend on H only through $\boldsymbol{J}$, when $\hat{\rho}$ is a free-electron-like resistivity tensor. This idea is supported by the limited data we have collected until now about current distributions in periodic composites [11]. However, we must now try to understand the radically different behavior of ρ_e in the 2D microstructures.

The first important observation is that, because there is a symmetry direction along which the material properties are constant—we shall always take this to be the x-direction—therefore both the electric field $\boldsymbol{E}(\boldsymbol{r})$ and the current density $\boldsymbol{J}(\boldsymbol{r})$ are independent of x except, possibly, near the system surface ∂V. This result, which seems obvious intuitively, can also be obtained in a more rigorous fashion from (1.3).

From the fact that $\nabla \times \boldsymbol{E} = 0$, it then follows that the x-component of $\boldsymbol{E}$ is constant everywhere (again, with the possible exception of regions near the surface). By contrast, the other components of $\boldsymbol{E}$, as well as all the components of $\boldsymbol{J}$, will in general depend in a non-trivial fashion upon y and z. Using these facts we shall now argue that, even though J_y and J_z may saturate as $|H| \to \infty$, J_x will usually not exhibit such behavior.

Consider a wire-like 3D system (i.e., it has a cross section with constant area and shape) with a 2D microstructure, whose symmetry axis x is perpendicular to the wire axis, which lies in the y, z-plane. The z-axis is taken to lie along the $\boldsymbol{B}$-field, therefore the volume-averaged current density $\langle \boldsymbol{J} \rangle$, which is directed along the wire, lies somewhere in the y, z-plane (see Fig. 7A). The local resistivity tensor is assumed to be free-electron-like everywhere, i.e.,

$$\hat{\rho} = \rho_0 \begin{pmatrix} 1 & -H & 0 \\ H & 1 & 0 \\ 0 & 0 & 1 \end{pmatrix}, \tag{2.2}$$

where ρ_0 represents the ohmic resistivity. Because the constant value of E_x satisfies

$$E_x = \rho_0 (J_x - H J_y), \tag{2.3}$$

therefore we can average E_x/ρ_0 to get

$$\left\langle \frac{1}{\rho_0} \right\rangle E_x = -\langle H J_y \rangle, \tag{2.4}$$

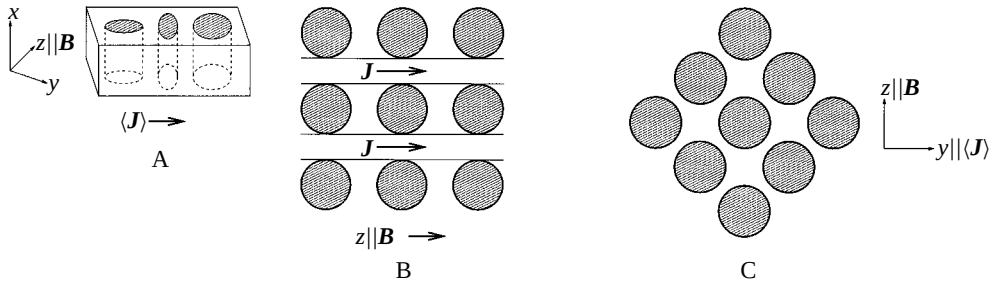

Fig. 7. A, Wire-shaped composite conductor. B, Current distribution when $\langle \boldsymbol{J} \rangle$ and $\boldsymbol{B}$ both lie along the principal axis z of a square array of cylindrical inclusions, and $|H| = |\mu \vec{B}| \gg 1$. Only $J_z(\boldsymbol{r})$ is non-zero, and its value is constant in the empty slab-shaped regions parallel to the z-axis. It vanishes in the complementary slab-shaped regions, which are defined by the parallel rows of cylindrical inclusions. C, Portion of a square array of cylinders (hatched), showing the directions of $\langle \boldsymbol{J} \rangle$ and $\boldsymbol{B}$ for the saturated minimum of $\tilde{\rho}_{\perp}^{(e)}$ in Fig. 5C. In the non-hatched regions in between the inclusions, $J_y(\boldsymbol{r})$ must be uniform when $|H| = |\mu \vec{B}| \gg 1$.

$$J_x = H J_y - \langle H J_y \rangle \frac{1/\rho_0}{\langle 1/\rho_0 \rangle}, \tag{2.5}$$

where we used the fact that $\langle J_x \rangle = 0$. Clearly, even if J_y is saturated, the magnitudes of both E_x and J_x will usually continue to increase with $|H|$, and therefore with $|\boldsymbol{B}|$.

An interesting particular case is that of a two-component mixture where component no. 1 (the inclusions) is a perfect insulator $\rho_0^{(1)} = \infty$. In that case, we can integrate (2.3) over V_2, the subvolume of component no. 2 (the host), to get

$$E_x = -\frac{1}{p_2} H_2 \rho_0^{(2)} \langle J_y \rangle, \tag{2.6}$$

$$J_x = H_2 \left(J_y - \frac{1}{p_2} \langle J_y \rangle \right), \qquad \boldsymbol{r} \in V_2, \tag{2.7}$$

where $p_2 = V_2/V$ is the volume fraction of component no. 2. Note that the integral of $\boldsymbol{J}$ over V_2 is the same as its integral over the entire volume, since $\boldsymbol{J} \equiv 0$ outside V_2.

By using (2.3) to substitute J_x into (2.1), the local rate of dissipation, which is non-zero only inside V_2, can be written there as

$$W = \frac{E_x^2}{\rho_0^{(2)}} + 2 H_2 E_x J_y + \rho_0^{(2)} [(1 + H_2^2) J_y^2 + J_z^2]. \tag{2.8}$$

Integrating this expression over V_2, recalling that $\boldsymbol{J} = 0$ outside V_2, and using (2.6), we finally get

$$\frac{\langle W \rangle}{\rho_0^{(2)}} = H_2^2 \left(\langle J_y^2 \rangle - \frac{1}{p_2} \langle J_y \rangle^2 \right) + \langle J_y^2 \rangle + \langle J_z^2 \rangle. \tag{2.9}$$

The first term on the r.h.s. is non-negative, since by the Cauchy–Schwartz inequality we have

$$V_2 \int_{V_2} dV\, J_y^2 \geq \left(\int_{V_2} dV\, J_y \right)^2. \tag{2.10}$$

Therefore, even if J_y and J_z become saturated, $\langle W \rangle$ will usually continue to increase as $H_2^2 \propto |\boldsymbol{B}|^2$. The only way to make $\langle W \rangle$ saturate is to have J_y uniform throughout V_2. Only in that case will the term in brackets in (2.9) vanish.

From the numerical results shown in Fig. 5, it appears that $\langle W \rangle$ indeed gets saturated for both $\langle \boldsymbol{J} \rangle \| \boldsymbol{B}$ and

$\langle \boldsymbol{J} \rangle \perp \boldsymbol{B}$, when $\boldsymbol{B}$ is in a direction where $\langle W \rangle$ has a minimum and H_2 or $|\boldsymbol{B}|$ is large enough. The inescapable conclusion is that at those points J_y must have a constant value over the subvolume V_2, or at least that $\langle J_y^2 \rangle - \langle J_y \rangle^2 / p_2$ is very small.

In the case where $\langle J_y \rangle = 0$, i.e., $\langle \boldsymbol{J} \rangle \| \boldsymbol{B}$, saturation of $\langle W \rangle$ requires that also $\langle J_y^2 \rangle = 0$, namely, that $J_y = 0$ everywhere. It follows that $J_x \equiv E_x \equiv 0$ too, and, therefore, that the current lines must all be straight and parallel to $\boldsymbol{B}$. Consequently, J_z must be limited to parallel slabs, as shown in Fig. 7B, and it must be *uniform there*! This means that we can calculate $\langle J_z^2 \rangle$ from a knowledge of $\langle J_z \rangle$, leading to the following result for the bulk effective longitudinal resistivity at the points (minima) where it is saturated:

$$\frac{\rho_{\|}^{(e)}}{\rho_0^{(2)}} = \frac{\langle W \rangle}{\langle \boldsymbol{J} \rangle^2 \rho_0^{(2)}} = \frac{\langle J_z^2 \rangle}{\langle J_z \rangle^2} = \frac{1}{p_{ac}}, \tag{2.11}$$

where p_{ac} is the (active) volume fraction of the current-carrying slabs. When $\boldsymbol{B}$ and $\langle \boldsymbol{J} \rangle$ are along the (100)-like directions, we have $p_{ac} = 1 - 2a$ (a is the cylinder radius, 1 is the edge length of the square unit cell), and this leads to reasonable agreement of (2.11) with the values of $\rho_{\|}^{(e)}/\rho_0^{(2)}$ at the saturated minima in those directions—see Figs 5B, E, and H. In the directions of the other minima, p_{ac} has smaller values—those are consistent with the larger values of $\rho_{\|}^{(e)}/\rho_0^{(2)}$ at those minima, some of which are unsaturated (i.e., (2.11) then provides an upper bound on the actual value at the minimum). We note that a strict step-function structure of J_z, as described here, is of course inconsistent with $J_y \equiv J_x \equiv 0$ for any finite value of H. Therefore, these results are approximate, but the approximation becomes better and better as $|H| \to \infty$.

In the case where $\langle J_z \rangle = 0$, i.e., $\langle \boldsymbol{J} \rangle \perp \boldsymbol{B}$, saturation of $\langle W \rangle$ requires that $\langle J_y^2 \rangle = \langle J_y \rangle^2 / p_2$. Therefore we get the following result for the bulk effective in-plane transverse resistivity (see the caption of Fig. 5 for the precise definition of $\tilde{\rho}_{\perp}^{(e)}$) at the points (minima) where it is saturated:

$$\frac{\tilde{\rho}_{\perp}^{(e)}}{\rho_0^{(2)}} = \frac{\langle W \rangle}{\langle J_y \rangle^2 \rho_0^{(2)}} = \frac{1}{p_2} + \frac{\langle J_z^2 \rangle}{\langle J_y \rangle^2}. \tag{2.12}$$

Obviously, $\rho_0^{(2)}/p_2$ is now a lower bound for $\tilde{\rho}_{\perp}^{(e)}$. That too is consistent with the values of $\tilde{\rho}_{\perp}^{(e)}/\rho_0^{(2)}$ at the minima in Fig. 5C, F and I. Like the previous results for the saturated minima of $\rho_{\|}^{(e)}$, these results are also approximate, but should become better and better as $|H| \to \infty$.

The conclusion that J_y must be uniform all over V_2 is unexpected and surprising, in view of the quite tortuous nature of that restricted volume, especially when the cylinder radii a are large (see Fig. 7C). How this comes about when $\boldsymbol{B}$ is large enough, and why it occurs only in low-order lattice symmetry directions, and only when a is small enough, is at present not understood. Another unexplained aspect of the rich phenomenology, of which Fig. 5 is an example, is the fact that there are low-order crystal symmetry directions for which $\tilde{\rho}_{\perp}^{(e)}$ has a saturated minimum when a is large. But as soon as a drops beneath a characteristic threshold for that particular direction, $\tilde{\rho}_{\perp}^{(e)}$ resumes its increase with H_2 and the saturated local minimum becomes an unsaturated local maximum (see Fig. 5C, F and I)!

In conclusion, the classical strong-field magnetotransport properties of periodic composites have proven to be a source of remarkable new phenomena and new modes of behavior. New phenomena are still being discovered and studied, almost entirely by resorting to theory and numerical calculations. There is clearly also a need for more experimental work on such systems before they are completely understood.

Acknowledgements—This research was supported, in part, by grants from the US–Israel Binational Science Foundation and the Israel Science Foundation. YMS was supported, in part, by the Gileadi Fellowship Program of the Ministry of Absorption of the State of Israel.

References

[1] M. Tornow, D. Weiss, K. v. Klitzing, K. Eberl, D. J. Bergman, and Y. M. Strelniker, Phys. Rev. Lett. **77**, 147 (1996).
[2] D. J. Bergman and Y. M. Strelniker, Phys. Rev. **B49**, 16256 (1994).
[3] J. R. Klauder and J. E. Kunzler, in *The Fermi Surface* edited by W. A. Harrison and M. B. Webb (New York, Wiley, 1960) p. 125.
[4] See, e.g., N. W. Ashcroft and N. D. Mermin, *Solid State Physics* (New York, Holt, Rinehart, and Winston, 1976) p. 292.
[5] D. J. Bergman and Y. M. Strelniker, Phys. Rev. **B51**, 13845 (1995).
[6] Y. M. Strelniker and D. J. Bergman, Phys. Rev. **B50**, 14001 (1994).
[7] R. Juretschke, R. Landauer, and J. A. Swanson, J. Appl. Phys. **27**, 838 (1956).
[8] D. Stroud and D. J. Bergman, Phys. Rev. **B30**, 447 (1984).
[9] A. K. Sarychev, D. J. Bergman, and Y. M. Strelniker, Phys. Rev. **B48**, 3145 (1993).
[10] D. J. Bergman, Physica Scripta **T49**, 655 (1993).
[11] Y. M. Strelniker and D. J. Bergman, Phys. Rev. **B53**, 11051 (1996).